

Use of Probabilistic Neural Network and Post Stack Inversion to Predict Reservoir Characterization in the Mediterranean Sea, Sapphire Field, Egypt

Ahmed Abosalama*

Department of Geology, Desert Research Center, Mathaf El Matariya, El Matariya, Cairo, Egypt

ABSTRACT

Geophysical parameters of probable reserves are interpreted using seismic inversion. It is essential for estimating porosity, saturation, and shale content. This article discusses the use of model-based Geophysical parameters of potential reserves are interpreted using seismic inversion. It is essential for determining porosity, saturation, and shale content. This article explores the use of model-based seismic inversion and probabilistic neural networks to characterize reservoirs. To make this assignment easier, the paper is divided into two portions. From 3D seismic data gathered in the research area (Sapphire Deep Seismic-2010), model-based inversion is used to generate acoustic impedance values. Seismic data is used to analyse five well logs. The average correlation coefficient between synthetic and seismic data is 0.997, with a 7% error, indicating the utility of model-based inversion. Second, a Probabilistic Neural Network (PNN) is trained and verified using estimated effective porosity, water saturation, and shale volume. The 3D variations in effective porosity, water saturation, and shale volume are obtained using the validated probabilistic neural network.

Our research revealed an undrilled section in the Sapphir-80 channel with favourable petro physical parameters, indicating a large volume of gas and condensate.

Seismic inversion connects observed seismic data to interpreted elastic physical parameters of probable reserves. Post-stack seismic inversion is used to estimate reservoir parameters such as porosity, saturation, shale content, etc. An application of model-based seismic inversion and probabilistic neural network to post-stack seismic data for reservoir characterization is described. The paper is divided into two pieces for this assignment. Initial post-stack seismic inversion approximating the Acoustic Impedance (AI) values using 3D seismic data recorded in the research area (Sapphire Deep Seismic-2010) in the time domain. Seismic data from five wells was gathered. As shown by 0.997 average correlation coefficient and 7% error between synthetic and seismic data, model-based inversion is effective. Second, a Probabilistic Neural Network (PNN) is trained and validated using data from the well sites. On the seismic volume, the probabilistic neural network calculates effective porosity, water saturation, and shale volume fluctuation in 3D.

The current analysis projected an undrilled area in the Sapphir-80 channel with good petro physical parameters, indicating a large volume of gas and condensate.

Keywords: Post stack inversion; Probabilistic Neural Network; Sapphire Field; Mediterranean

INTRODUCTION

Seismic inversion recovers earth properties from seismic data. A wavelet, an initial earth model, and TWT horizons are required for seismic inversion [1]. Seismic inversion for hydrocarbon detection has grown steadily over the last two decades. Seismic inversion and log data help extract subsurface petro-physical properties (porosity, shale volume, acoustic, elastic, and density) [2]. Post-Stack seismic

inversion is used to extract acoustic impedance and establish a relationship between impedance and petro-physical properties. Geophysical applications of neural networks date back to the early 1990s. McCormack, et al. [3], used back propagation Multi-Layer Feed Forward Networks to predict lithology log for an entire well (MLFN). Recently, Probabilistic Neural Networks (PNN) has proven to be a reliable predictor of reservoir parameters such as porosity [4,5]. PNNs have also been used to detect hydrocarbon migration

Correspondence to: Ahmed Abosalama, Department of Geology, Desert Research Center, Mathaf El Matariya, El Matariya, Cairo, Egypt, Tel: +2023456772345; E-mail: ahmed.abosalama.850@gmail.com

Received: 25-Jul-2022; Manuscript No. JGG-22-16209; **Editor assigned:** 28-Jul-2022; PreQC. No. JGG-22-16209 (PQ); **Reviewed:** 11-Aug-2022; QC. No. JGG-22-16209; **Revised:** 18-Aug-2022; Manuscript No. JGG-22-16209 (R); **Published:** 26-Aug-2022, DOI: 10.35248/2381-8719.22.11.1042.

Citation: Abosalama A (2022) Use of Probabilistic Neural Network and Post Stack Inversion to Predict Reservoir Characterization in the Mediterranean Sea, Sapphire Field, Egypt. J Geol Geophys. 11:1042.

Copyright: © 2022 Abosalama A. This is an open-access article distributed under the terms of the Creative Commons Attribution License, which permits unrestricted use, distribution, and reproduction in any medium, provided the original author and source are credited.

patterns and traps [6,7]. The PNN algorithm has the ability to build nonlinear relationships between petro-physical logs and seismic data. Thus, it can be used to accurately predict reservoir properties in 3D volumes. In the Sapphire gas field, Offshore Nile Delta, we used PNN to predict reservoir petro-physical properties from seismic data. The impedance volume becomes reservoir parameters (effective porosity, water saturation and shale volume volumes).

Geological setting

The Nile Delta is located on the northern edge of the African Plate and is structurally important in the development of the eastern Mediterranean and Levant basins. The region in Lower Egypt where the Nile River extends out and empties into the Mediterranean Sea is known as the Nile Delta. It spans 240 km of the Mediterranean coastline, from Alexandria in the west to Port Said in the east,

and is one of the largest river deltas in the world. It is also a rich agricultural zone. The delta is roughly 160 km long from north to south. From Cairo, the Delta extends slightly downstream. According to Abdel Aal, et al. [8], this basin's current structure is defined by six major structural trends that shaped its Neogene successions. The NW Tensah structural trend, the NE Rosetta fault trend, the Pelusim shear zone, the minor NS Baltim fault trend, and the NW Red Sea–Gulf of Suez fault trend. These fold axes were created by Rosetta and Tensah transgressive movements during the Early–Middle Miocene [9]. The Sapphire gas field is located in the 152 km² West Delta Deep Marine concession (Figure 1). The sapphire field is linked to the NDO Anticline, which runs parallel to the NE Rosetta fault trend (Figure 2). The reservoir target in Sapphire field is deep marine basin floor fans and slope channel sands in the Kafr El Sheikh formation (Figure 3).

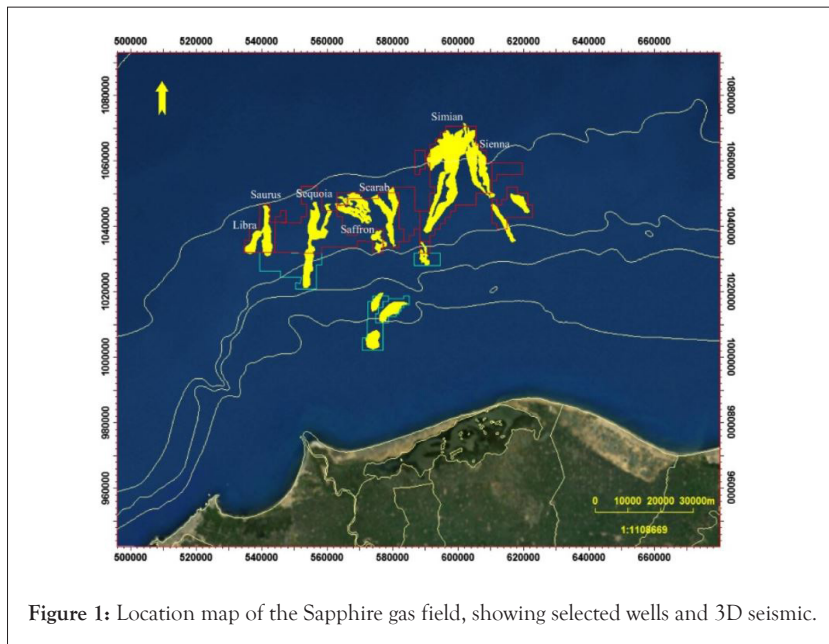


Figure 1: Location map of the Sapphire gas field, showing selected wells and 3D seismic.

AGE	STAGE	BIOZONES	FORMATION	LITHOLOGY	RESER. S. ROCK	MAIN FIELD	SEQUENCE STRATIGRAPHY ONLAP CURVE	
HOLOCENE	LATE	N-23	NN-21	EL MUGHARBI				
		MI-23	NN-20	EL MUGHARBI				
	EARLY	MI-22	NN-19	EL WASTANI				
		MI-21	NN-18	EL WASTANI				
	MIOCENE	LATE	PI-21	NN-17	EL WASTANI			
			PI-20	NN-16	EL WASTANI			
			PI-19	NN-15	EL WASTANI			
			PI-18	NN-14	EL WASTANI			
			PI-17	NN-13	EL WASTANI			
		EARLY	PI-16	NN-12	KAFR EL SHEIKH			
PI-15			NN-11	KAFR EL SHEIKH				
PI-14			NN-10	KAFR EL SHEIKH				
PI-13			NN-9	KAFR EL SHEIKH				
PI-12			NN-8	KAFR EL SHEIKH				
MIOCENE	UPPER	MI-11	NN-7	ABU MADI				
		MI-10	NN-6	ABU MADI				
		MI-9	NN-5	ABU MADI				
		MI-8	NN-4	ABU MADI				
		MI-7	NN-3	ABU MADI				
	MIDDLE	MI-6	NN-2	QANTARA				
		MI-5	NN-1	QANTARA				
		MI-4	NN-0	QANTARA				
		MI-3	NN-0	QANTARA				
		MI-2	NN-0	QANTARA				
LATE	MI-1	NN-0	TINEH / DABA					
	MI-0	NN-0	TINEH / DABA					

Figure 2: Nile Delta stratigraphic column and hydrocarbon system. Modified from Rio et al. (1991) showing the study interval. Note: (Yellow) Sandston (Green) Shale-clay (Pink) Evaporites (Grey) Hiatus/Erosion (Black Triangle) Sourcerock (Black Circle) Oil and Gas (Red Star) Gas.

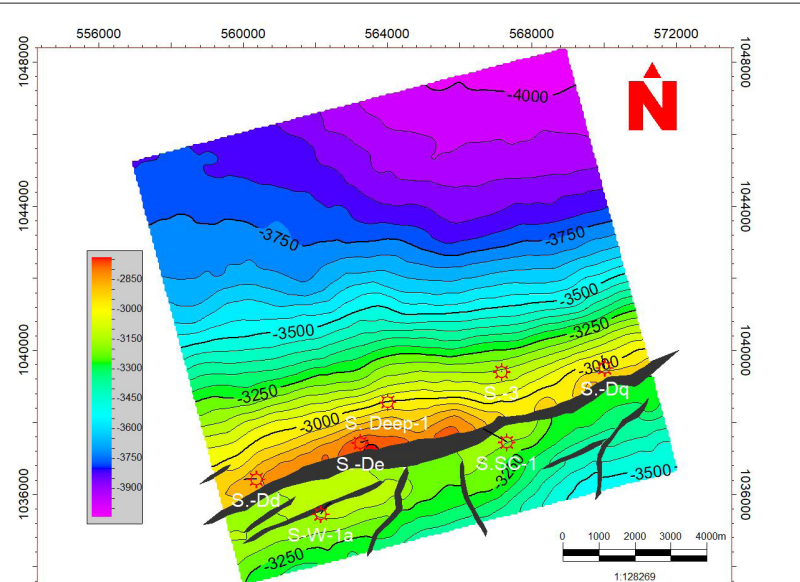


Figure 3: Depth Structure contour map, Sapphire-80 Formation in Sapphire field, showing ENE-WSW trending NDOA anticline that is dissected by three fault trends (ENE-WSW, NE-SW, and N-S).

MATERIALS AND METHODS

In applications involving classification and pattern recognition, Probabilistic Neural Networks (PNNs) offer a scalable substitute for traditional back-propagation neural networks. They do not require the intensive forward and reverse computations that conventional neural networks require. They can also use other forms of training data. When used to solve a classification problem, these networks use the idea of probability theory to reduce the number of incorrect classifications. PNN is frequently employed in classification techniques. The first layer calculates the separation between the input vector and the training input vectors when an input is present. The result is a vector whose components represent how similar the input is to the training input. The second layer generates its net output as a vector of probabilities by adding the contributions from each type of inputs. Finally, compete transfer function on the output of the second layer selects the highest of these probabilities, resulting in a 1 (positive identification) for that class and a 0 (negative identification) for classes that are not targeted.

Reconstructing earth properties is done by a process called seismic inversion, which is typically employed in the oil and gas industries. It combines seismic and well data to anticipate rock attributes (lithology, fluid content, and porosity) throughout a survey. These characteristics of the rock can be used to pinpoint the reservoir and hydrocarbon. The two types of seismic inversion procedures are post-stacking and pre-stacking inversion. The most commonly used method for inversion is the first technique, known as post-stacking inversion. Using seismic data, well data, and a fundamental understanding of stratigraphy for interpretation, this method converts a single seismic information volume into an acoustic impedance volume. By eliminating the wavelet from seismic data, we contribute to the production of a high-resolution image of the subsurface. In general, "post stack inversion procedures" refers to a range of processes for converting stacked seismic data into quantifiable rock physics parameters. Acoustic impedance is often the product of post stack inversion, but pre-stack inversion may produce both acoustic and shear impedance. Sparse spike inversion, model-based inversion, recursive inversion, and colored

inversion are examples of post-stack inversion techniques. Due to the absence of probabilistic metrics, these techniques are always categorized as deterministic techniques.

RESULTS AND DISCUSSION

The data used in the study are 3D seismic cube (Sapphire Deep Seismic-2010) and well logs from six wells (Sapphire South Central-1, Sapphire-Dq, Sapphire-Deep-1, Sapphire-De, Sapphire-Dd and Sapphire-3). It includes P-wave, density, SW, Vcl, and effective porosity. Specifically, we used post-stack inversion and neural network analysis. The first step was to convert 3D seismic data to acoustic impedance. This study uses a deterministic wavelet (Figure 4) generated by convolving P-wave and density log reflectivity series with well log wavelet data. The log-to-seismic correlation (Figure 5) and horizons (top Sapphire-40, 60, 70, 80) were then selected (Table 1). A model was constructed by inversion (Figures 6-8). In this first model, we add the missing low and high frequencies Modified initial models to improve fit between actual seismic traces and synthetic traces and reduce errors. There is a 97% average correlation between synthetic and seismic data in this inversion. Synthetic and seismic data are highly correlated at the Sapphire south-central well location (Table 2), and actual and inverted P-impedance logs are highly correlated (Figure 9). This confirms model-based inversion. Inversion of the post-stack yields Z_p volume (Figure 10). A geo-statistical model can predict many petro-physical parameters from well and seismic data. Using probabilistic neural networks, effective porosity and shale content are calculated. The logs were effective porosity, water saturation, and shale content. Input data include a 3D seismic cube, inverted results (Z_p volume), envelop, RMS, and sweetness volumes. To use a neural network to estimate porosity in a 3D volume, first train it on seismic and measured log data (Figures 10-12). The relationship is then applied to the entire volume. To find the number of operators and attributes, we use the multi-attribute (Figures 13-15). If we accept the multi-attribute method analysis, we can use PNN to predict SW, and Vsh at the well locations (Figures 16-18) and test the process using cross plots (Figures 19-21) between actual SW, and predicted SW, and Saturation, effective porosity, and shale content volumes were generated using PNN (Figures 22-25).

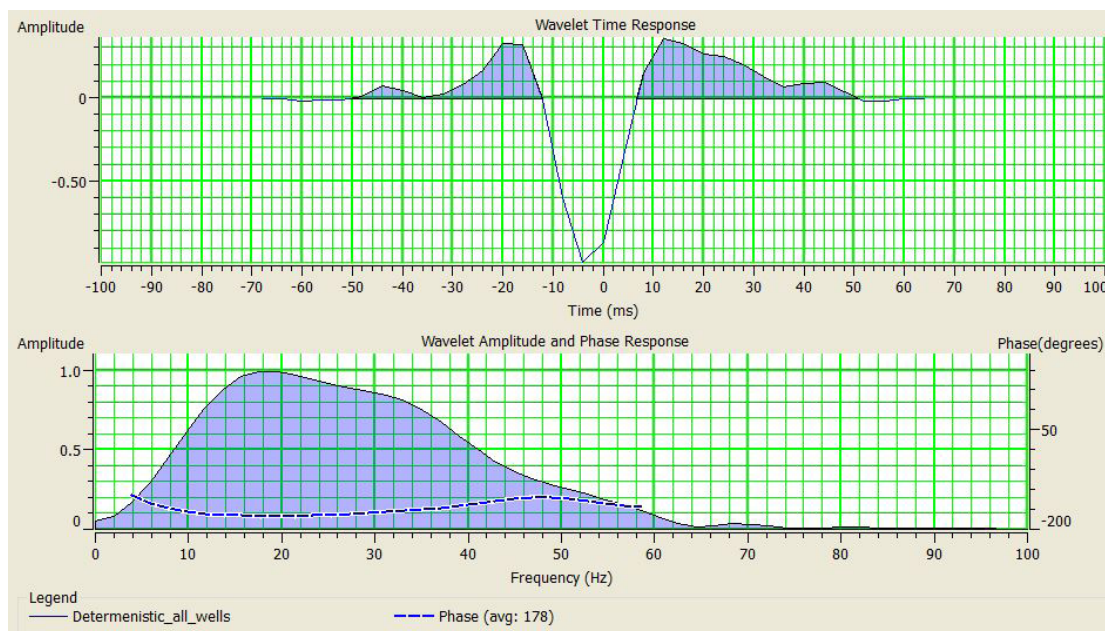


Figure 4: Deterministic wavelet using five wells used in this study with time response on top and respective amplitude spectrum on the bottom. The phase is constant 180 degree. **Note:** (—) Deterministic all wells, (---) Phase (avg: 178)

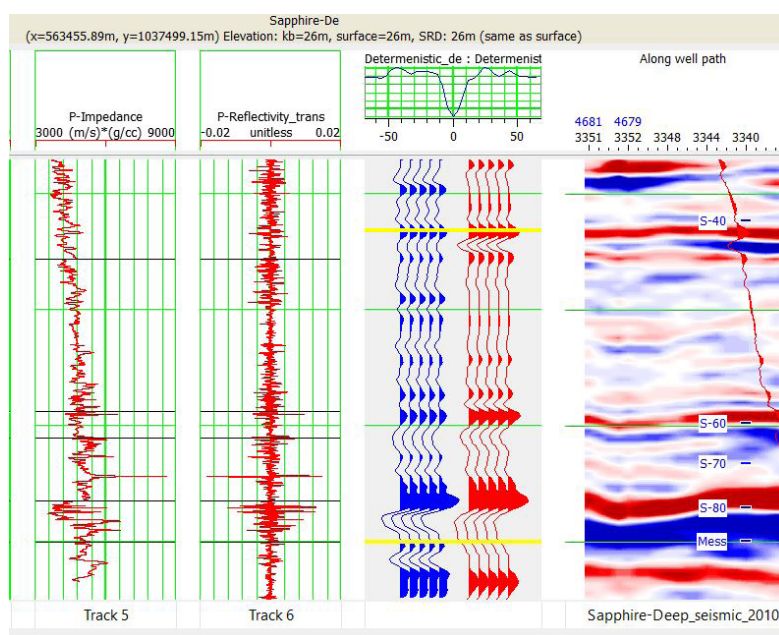


Figure 5: An example of the well ties in Sapphire De well using deterministic wavelet. The logs (from left to right) are, P-impedance (IP), and reflectivity. The blue seismic trace is the calculated synthetic, and the red is the real seismic data respectively.

Table 1: The correlation coefficients of the five wells using both statistical wavelets and deterministic wavelets.

Well	Wavelet correlation coefficient	
	Statistical	Deterministic
Sapphire South Central-1	0.703	0.859
Sapphire-Dq	0.7	0.816
Sapphire-Deep-1	0.892	0.905
Sapphire-De	0.821	0.871
Sapphire-3	0.768	0.856
Average	0.777	0.87
0, 654	0, 654	0, 654

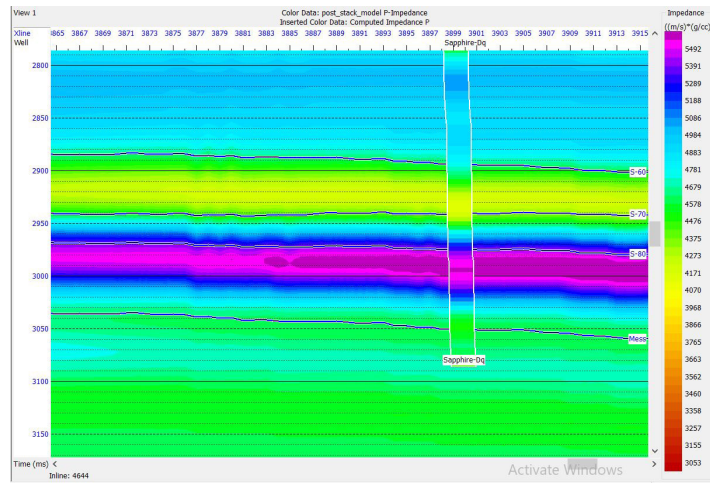


Figure 6: Initial Acoustic Impedance (AI) model of In-line 4644. showing the actual impedance for Sapphire Dq well compared to the initial model impedance.

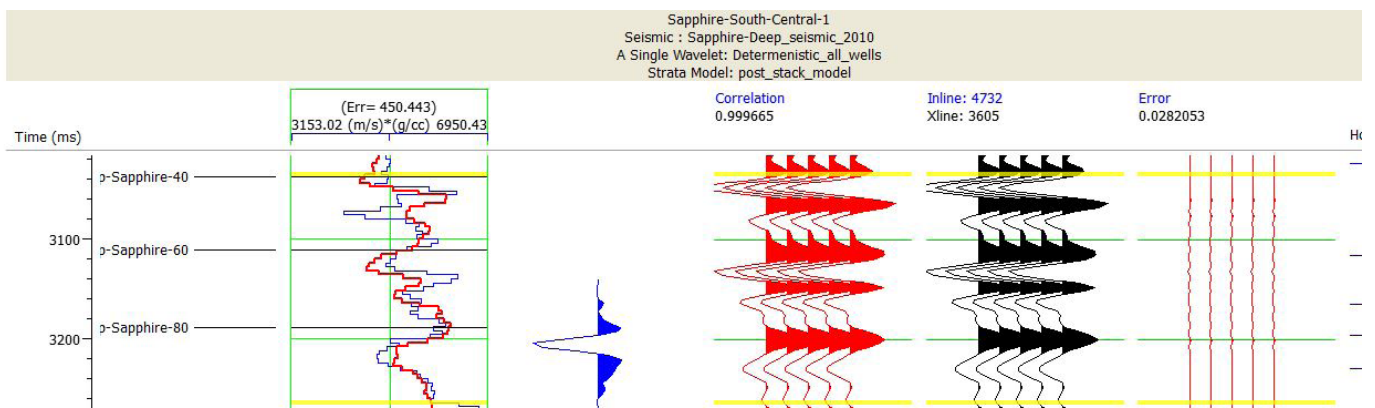


Figure 7: Post-stack inversion analysis for well Sapphire South Central using deterministic wavelet. Showing the inversion analysis was done for the reservoir interval in Sapphire 40 to Sapphire 80.

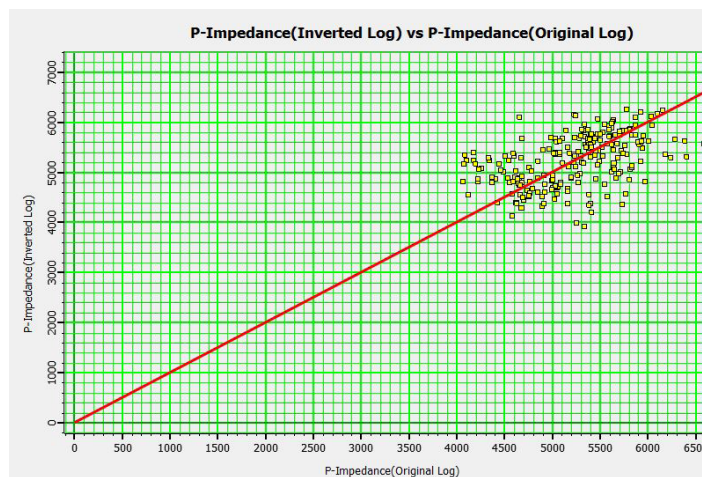


Figure 8: Cross plot illustrates P-impedance of Inversion results versus the P-impedance of actual log data. P. Showing the linear relation between Inversion results and actual log data.

Table 2: Error values between the inverted and the original well logs and the correlation coefficients between the original and synthetic seismic data.

Well	Correlation coefficient	Synthetic error
Sapphire South Central-1	0.9996	0.0282
Sapphire-Dq	0.9983	0.0659
Sapphire-Deep-1	0.9982	0.0618
Sapphire-De	0.9953	0.0991
Sapphire-3	0.9954	0.0982

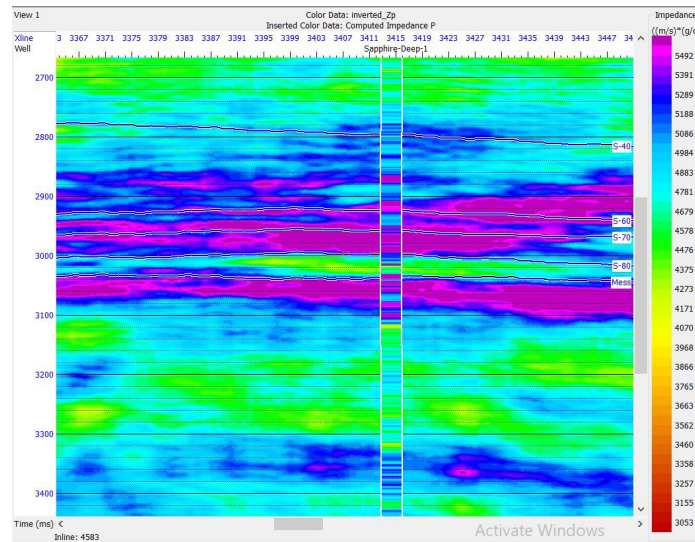


Figure 9: Inline Seismic section for post-stack inversion results showing p-impedance (Z_p) with p-impedance log curves at Sapphire Deep-1 well.

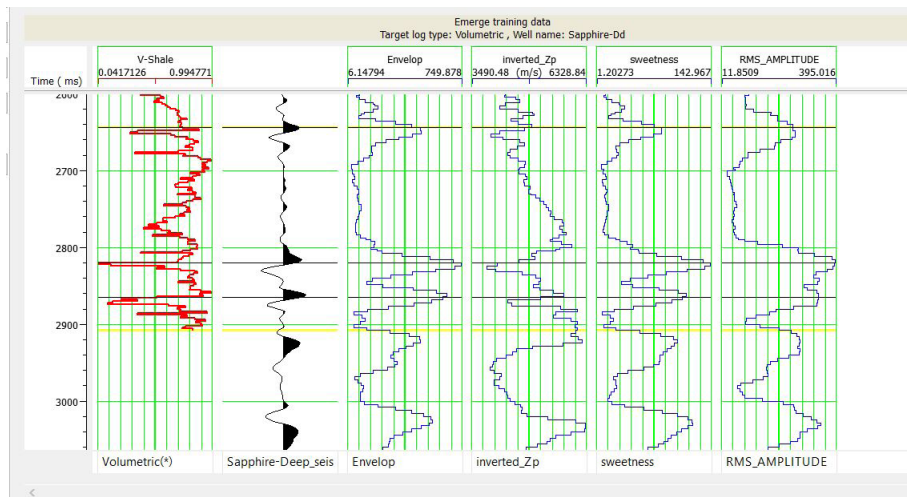


Figure 10: Analysis of target log (red) shale content, seismic trace (black) Sapphire Dd, external attribute volumes trace (blue) and analysis window (horizontal yellow lines).

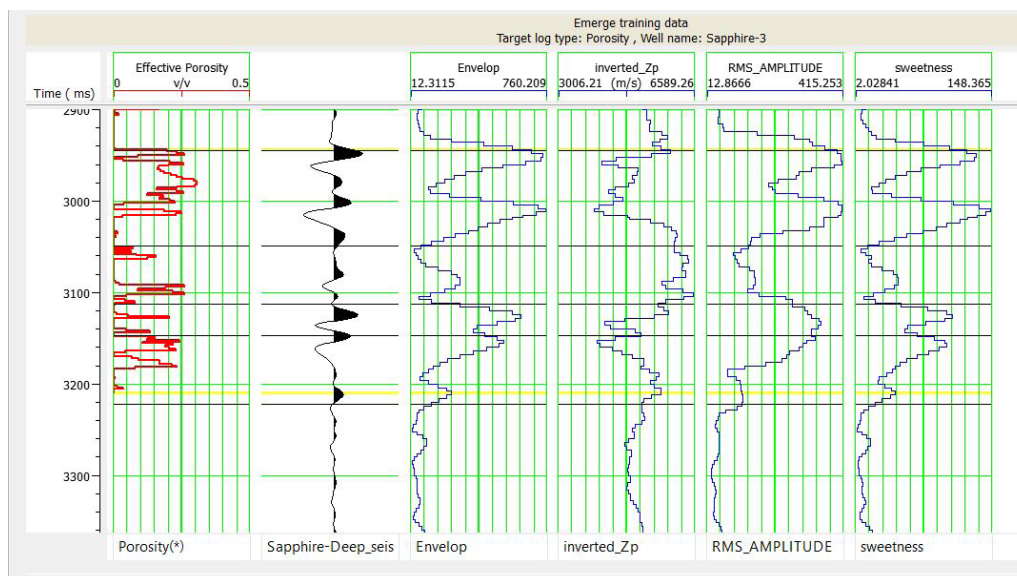


Figure 11: Analysis of target log (red) porosity, seismic trace (black) Sapphire Deep-1, external attribute volumes trace (blue) and analysis window (horizontal yellow lines).

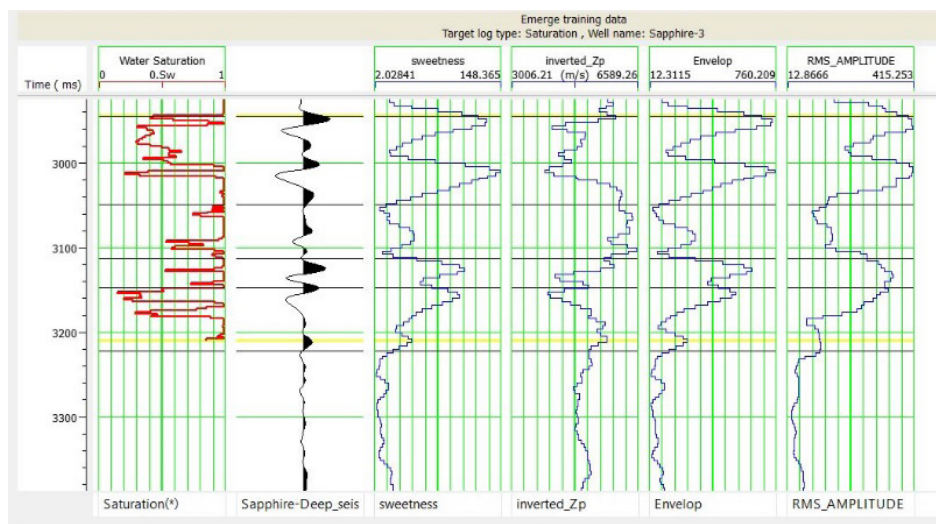


Figure 12: Analysis of target log(red) water saturation, seismic trace(black) Sapphire-3, external attribute volumes trace (blue) and analysis window (horizontal yellow lines).

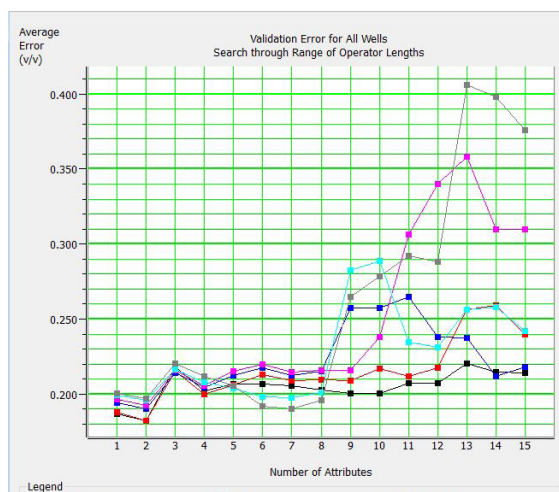


Figure 13: Validation error plot for different operator lengths. The minimum validation error occurs when a three-point operator (red curve) is used with two attributes. Note: (—■—) 1 point, (—■—) 3 point, (—■—) 5 point, (—■—) 7 point, (—■—) 9 point, (—■—) 11 point.

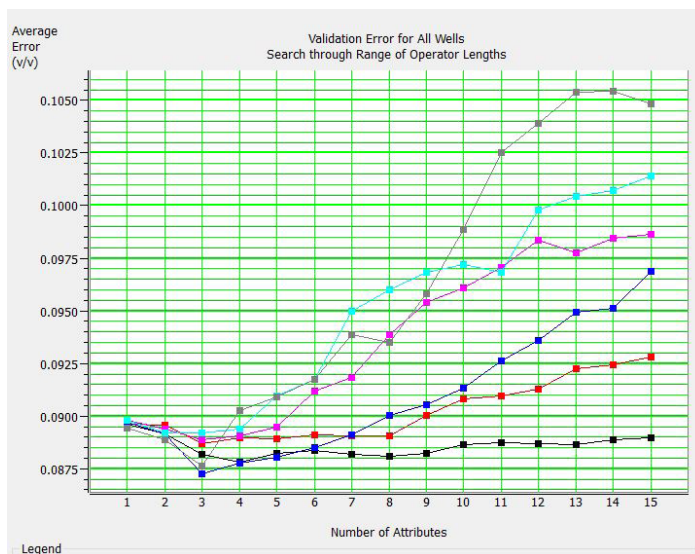


Figure 14: Validation error plot for different operator lengths. The minimum validation error occurs when a three-point operator (red curve) is used with two attributes. Note: (—■—) 1 point, (—■—) 3 point, (—■—) 5 point, (—■—) 7 point, (—■—) 9 point, (—■—) 11 point.

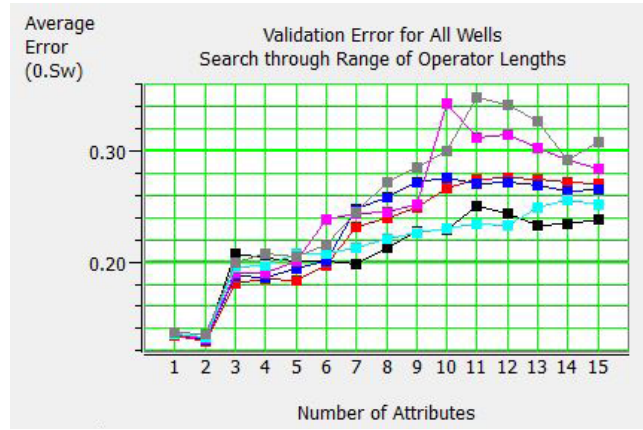


Figure 15: Validation error plot for different operator lengths. The minimum validation error occurs when a three-point operator (red curve) is used with six attributes. Note: (—■—) 1 point, (—■—) 3 point, (—■—) 5 point, (—■—) 7 point, (—■—) 9 point, (—■—) 11 point.

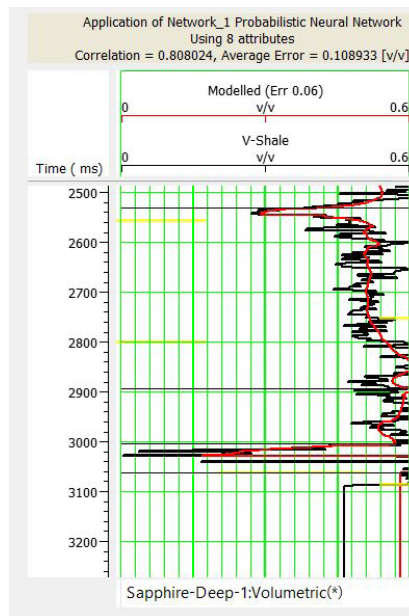


Figure 16: The application of the PNN for Vsh prediction. Measured logs are shown in black and the predicted ones are shown in red.

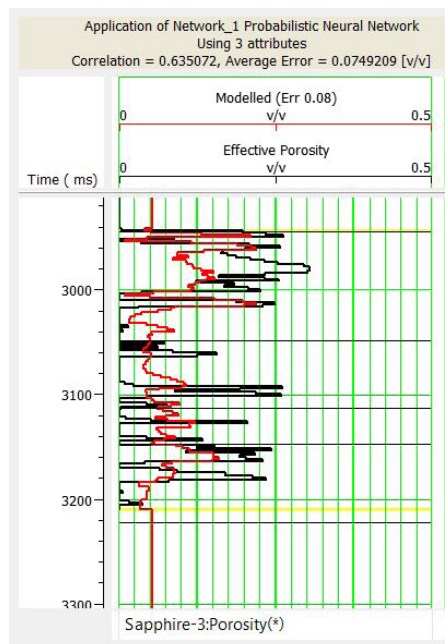


Figure 17: The application of the PNN for effective porosity prediction. Measured logs are shown in black and the predicted ones are shown in red.

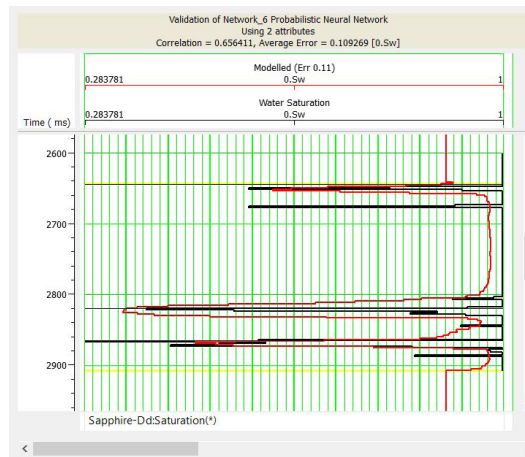


Figure 18: The application of the PNN for water saturation prediction. Measured logs are shown in black and the predicted ones are shown in red.

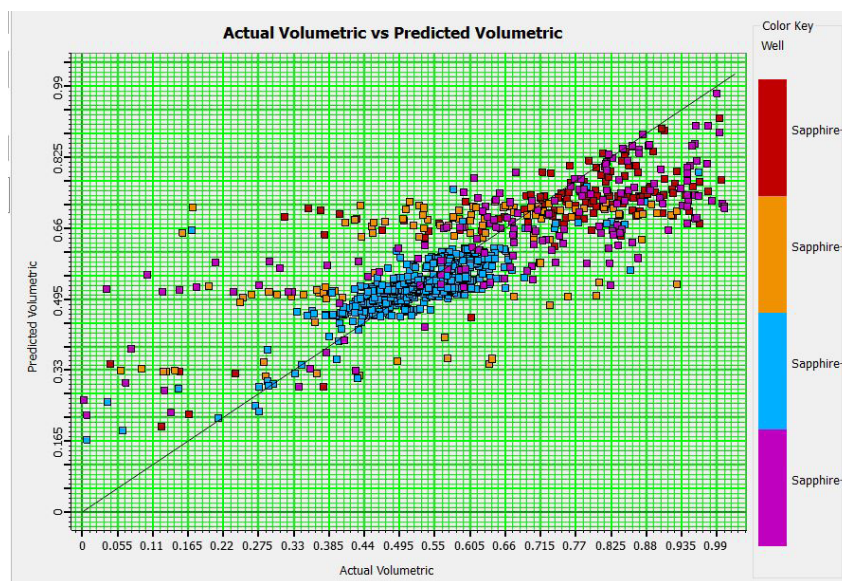


Figure 19: Relationship between the actual and predicted shale content. Note: Colour key well, (red) Sapphire, (orange) Sapphire, (blue) Sapphire, (purple) Sapphire.

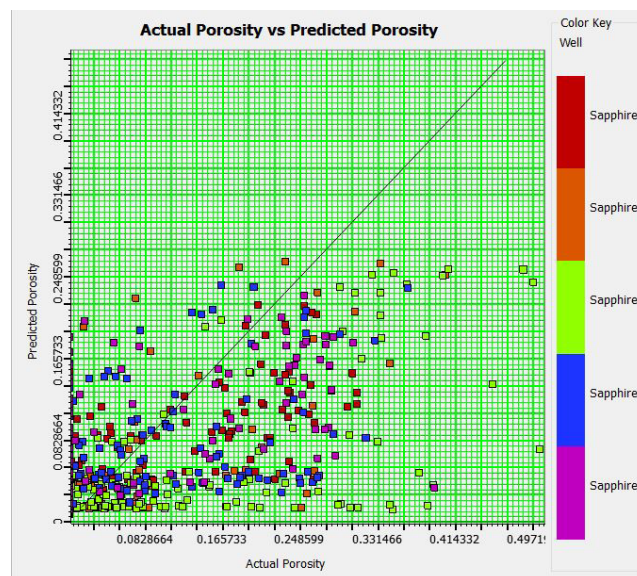


Figure 20: Relationship between the actual and predicted effective porosity. Note: Colour key well, (red) Sapphire, (orange) Sapphire, (green) Sapphire, (blue) Sapphire, (purple) Sapphire.

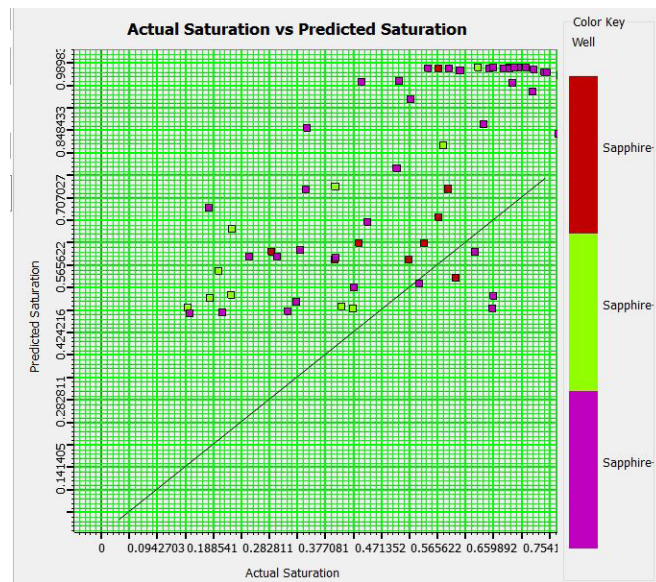


Figure 21: Relationship between the actual and predicted waater saturation. Note: Colour key well, (red) Sapphire, (green) Sapphire, (purple) Sapphire.

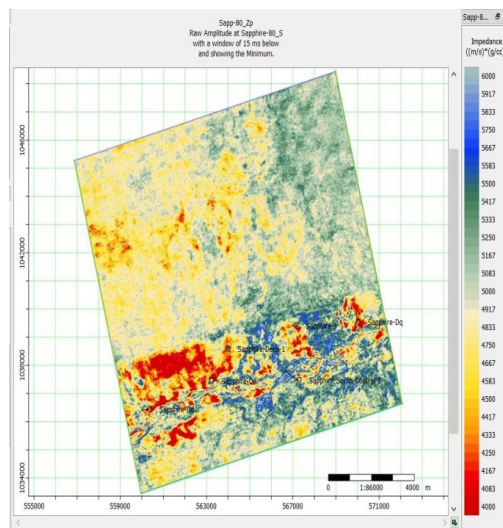


Figure 22: Relative P-Impedance slice (RMS Amplitude) on Sapphire-80. There is undrilled low amplitude part (sand reservoir) that takes Sheet shape.

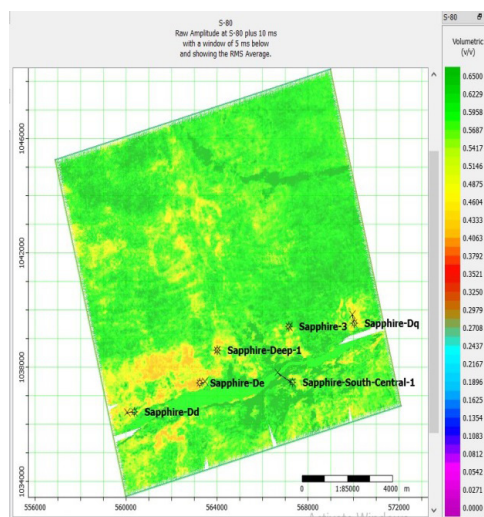


Figure 23: Relative P-Impedance slice (RMS Amplitude) on Sapphire-80. There is undrilled low shale content part (sand reservoir) that takes Sheet.

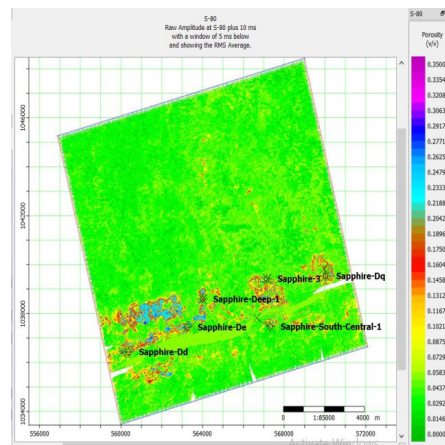


Figure 24: Relative P-Impedance slice (RMS Amplitude) on Sapphire-80. There is undrilled high effective porosity (sand reservoir) that takes Sheet shape.

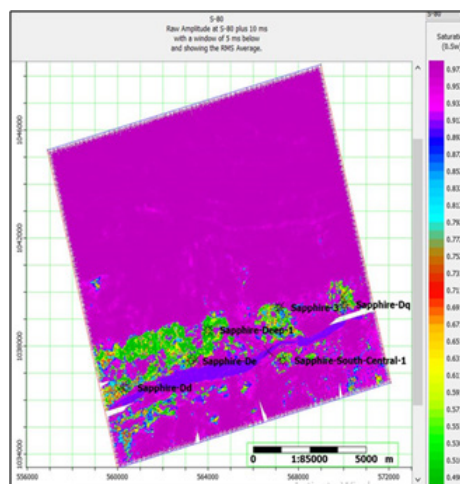


Figure 25: Relative P-Impedance slice (RMS Amplitude) on Sapphire-80. There is undrilled low water saturation (sand reservoir) that takes Sheet shape.

CONCLUSION

According to the findings of this study, the Sapphir-80 channel is oriented ENE-WSW along the NDO Anticline trend. Its width ranges from 1.2 km to 2 km, and its length is approximately 12 km. In the current study, we estimated an undrilled area with a good thickness and good petro physical parameters, implying that this area contains a significant volume of gas and condensate by using post-stack inversion followed by a probabilistic neural network approach. A geo-statistical model can predict many petro-physical parameters from well and seismic data. This study uses a deterministic wavelet generated by convolving P-wave and density log reflectivity series with well log wavelet data. Using probabilistic neural networks, effective porosity and shale content are calculated.

REFERENCES

1. Veeken PC, Da Silva AM. Seismic inversion methods and some of their constraints. *First Break*. 2004;22(6):47-70.
2. Maurya SP, Singh KH. Reservoir characterization using model based inversion and probabilistic neural network. *Discovery*. 2015;49(228):122-127.
3. McCormack MD. Neural computing in geophysics. *Lead Edge*. 1991;10(1):11-15.
4. Helle HB, Bhatt A, Ursin B. Porosity and permeability prediction from wireline logs using artificial neural networks: A North Sea case study. *Geophys Prospect*. 2001;49(4):431-444.
5. Cersósimo DS, Ravazzoli CL, Martínez RG. Prediction of lateral variations in reservoir properties throughout an interpreted seismic horizon using an artificial neural network. *Lead Edge*. 2016;35(3):265-269.
6. Clifford A, Aminzadeh F. Gas detection from absorption attributes and amplitude versus offset with artificial neural networks in Grand Bay Field. In *SEG Technical Program Expanded Abstracts*. Soc Explor Geophys. 2011;375-380.
7. Araya-Polo M, Dahlke T, Frogner C, Zhang C, Poggio T, Hohl D. Automated fault detection without seismic processing. *Lead Edge*. 2017;36(3):208-214.
8. Abdel Aal A, Price RJ, Vaitl JD, Shallow JA. Tectonic evolution of the Nile Delta, its impact on sedimentation and hydrocarbon potential. In *EGPC 12th exploration and production conference*. 1994;1:19-34.
9. Farouk S, Jain S, Abd-Elazez M, El Shennawy T, Shaker F. High resolution Pliocene–Pleistocene calcareous nannofossil distribution and palaeoenvironmental changes in the northwest Nile Delta, Egypt. *Lethaia*. 2021.